12-18-2007

Interfacial Coherency and Ferroelectricity of $BaTiO_3/SrTiO_3$ Superlattice Films

Y. L. Li
Pennsylvania State University

S. Y. Hu
Pacific Northwest National Laboratory

Dmitri Tenne
Boise State University

A. Soukiassian
Pennsylvania State University

D. G. Schlom
Pennsylvania State University

See next page for additional authors

Interfacial coherency and ferroelectricity of $BaTiO_3/SrTiO_3$ superlattice films

Y. L. Li

Department of Materials Science and Engineering, The Pennsylvania State University, University Park, Pennsylvania 16802, USA

S. Y. Hu

Materials Structure and Performance, Pacific Northwest National Laboratory, Richland, Wasington 99352, USA

D. Tenne

Department of Physics, Boise State University, 1910 University Drive, Boise, Idaho 83725, USA

A. Soukiassian and D. G. Schlom,

Department of Materials Science and Engineering, The Pennsylvania State University, University Park, PA 16802, USA

X. X. Xi

Department of Materials Science and Engineering, and Department of Physics, The Pennsylvania State University, University Park, Pennsylvania 16802, USA

K. J. Choi and C. B. Eom

Department of Materials Science and Engineering, University of Wisconsin, Madison, Wisconsin 53706, USA

A. Saxena and T. Lookman

T-11, Los Alamos National Laboratory, Los Alamos, New Mexico 87545, USA

Q. X. Jia

MPA-STC, Los Alamos National Laboratory, Los Alamos, New Mexico 87545, USA

L. Q. Chen

Department of Materials Science and Engineering, The Pennsylvania State University, University Park, Pennsylvania 16802, USA

We studied the phase transitions, domain morphologies, and polarizations in $BaTiO_3/SrTiO_3$ superlattices grown on $SrTiO_3$ substrates. Using the phase field approach, we discovered the remarkable influence of film/substrate interfacial coherency on the ferroelectricity of the $SrTiO_3$ layers within a superlattice: it is an orthorhombic ferroelectric for an incoherent interface while it exhibits only induced polarization by the adjacent $BaTiO_3$ layers for a coherent interface. We presented the domain morphologies within individual $BaTiO_3$ and $SrTiO_3$ layers which have different ferroelectric symmetries. The results are compared to ultraviolet Raman spectroscopy and variable temperature x-ray diffraction measurements.

Superlattices allow great flexibility for material design by tailoring the components and their layer thicknesses to produce striking property enhancements as well as new combinations of desired properties. Among the widely studied oxide superlattices, the $BaTiO_3$ (BT)/$SrTiO_3$ (ST) system has attracted the most attention because of its chemical stability and adaptive high dielectric constant.[1-14] Even so, the nature of ferroelectric phase transitions and ferroelectricity of BT/ST superlattices are still not well understood. For example, recent ultraviolet (UV) Raman measurements[12] and phase-field simulations[13] showed that although the ferroelectric transition temperature T_c of BT/ST superlattices on a ST substrate can be tuned by ~500 Kelvin by varying the thickness of the BT and ST layers, the ST layers within the superlattices only exhibit induced polarization.[13] On the other hand, other studies by Rios *et al*.,[6] Jiang *et al*.,[7] and Johnston *et al*.[11] indicated that the ST layers are ferroelectric with an orthorhombic symmetry. The main objective of this work is to understand the seemingly drastically different observations of ferroelectricity of BT/ST superlattices on a ST substrate from different sources.

Our fundamental hypothesis is that it is the lattice coherency between a BT/ST superlattice and its underlying ST substrate that largely controls the ferroelectricity of the ST layers within the superlattice. We employ the phase-field approach[15,16] and take the ferroelectric polarization, $\mathbf{P}=(P_1,P_2,P_3)$, as the order parameter. The evolution of $\mathbf{P}$ towards its equilibrium state is described by the time-dependent Ginzburg-Landau equations,

$$\frac{\partial P_i(\mathbf{x},t)}{\partial t}=-L\frac{\delta F}{\delta P_i(\mathbf{x},t)},\ (i=1,2,3), \tag{1}$$

where L is the kinetic coefficient related to the ferroelectric domain wall mobility, t is time, and $\mathbf{x}=(x_1,x_2,x_3)$ is the coordinate. F is the total free energy of the system, which includes the bulk chemical free energy, elastic energy, electrostatic energy, and gradient energy, i.e., $F=F_{bulk}(P_i)+F_{elas}(P_i,\varepsilon_{ij})+F_{elec}(P_i,E_i)+F_{grad}(P_{i,j})$, where ε_{ij} is the strain resulted from ferroelectric phase transition and constraint among the different layers and substrate, E_i is the electric field from dipole-dipole interactions, and $P_{i,j}=\partial P_i/\partial x_j$. The details and the numerical coefficients for obtaining the different energy contributions can be found in Ref. 13.

To investigate the effect of lattice coherency, we consider three superlattices of BT_8/ST_4 grown on (001) ST substrates, i.e., one period of the superlattice consists of 8 unit cells of $(001)_p$ oriented BT and 4 unit cells of $(001)_p$ oriented ST along the growth direction, where the subscript p denotes the pseudocubic unit cell. Superlattices (a), (b) and (c) are fully commensurate, partially relaxed and fully relaxed with the (001) ST substrate, respectively. The in-plane lattice parameters of the superlattices are given in Fig. 1.

We first discussed their ferroelectric transition temperatures. We identify the temperature below which there exists a spontaneous polarization as the transition temperature. The results are shown in Table I. The transition temperatures determined from UV Raman spectroscopy and the variable temperature x-ray diffraction (VTXRD) are also included in Table I for comparison. The experimental measurements were for the superlattices of ST_4/BT_8 with 10 periods (fully commensurate) and with 40 periods (partially relaxed), respectively.[12]

From the polarization distribution and domain structures, we found that under the fully commensurate and the partially relaxed conditions, both the ST layer and BT layer exhibit tetragonal symmetry with polarizations perpendicular to the superlattice planes. The polarization in ST layers was induced by the adjacent BT layers, i.e., ST layers are nonferroelectric. However, under the fully relaxed condition, the ST layer is ferroelectric with orthorhombic symmetry. Its polarizations are in-plane along the ST $[110]_p$ directions. It was reported that relaxed ST/BT superlattices may possess symmetries lower than tetragonal.[6,7,10,11,14] However, the tetragonal symmetry in the BT layer is still retained with the polarization along the out-of-plane direction. It should be noted that the BT layers are still under an in-plane compressive strain even though the superlattice is fully relaxed with respective to the (001) ST substrate. On the other hand, the ST layers are subjected to a tensile strain (~1.7%), and as it has been showed previously strained ST is ferroelectric.[17,18] The corresponding domain structure of the relaxed superlattice at room temperature is showed in Fig. 2. Going from BT to ST layers, the polarization rotates from ST $[001]_p$ toward ST $[110]_p$ direction with those near the interfaces along ST $[100]_p$ or $[010]_p$ directions.

Figure 3 (a-c) is the distributions of the polarization components (P_1,P_2,P_3) across the superlattice thickness at room temperature under the three constraints. The thicker lines with symbols (triangles, circles, squares) are the averages of the polarization components over the superlattice plane (the x_1x_2 plane). The other thinner lines are the polarization components from a cross section (parallel to x_2x_3 plane) of the superlattice. The out-of-plane component, P_3, always has a maximum in the middle of the BT layer irrespective of the constraints. But the magnitude of P_3 decreases with increasing

relaxation. The distributions of the in-plane components, P_1 and P_2, however, are very different under the three constraints. They are always zero at the middle of both BT and ST layers under the both fully commensurate and partially relaxed conditions. Under full relaxation, however, not only they are no longer zero but also their averages are maxima at the middle of the ST layer. We also notice that P_3 is not always zero in the ST layer. Our simulations demonstrate that it is a result of both the dipole-dipole interaction between the BT and ST layers and the gradient energy as P_3 is zero in ST layers for the three superlattices if the dipole-dipole interaction and the gradient energy are artificially switched off. This could be viewed as a "ferroelectric proximity" effect and has been discussed.[19,20]

Figure 4 shows the lattice parameters versus temperature for the superlattice of ST_4/BT_8 under fully commensurate constraint. The behavior is approximately linear at high temperatures, and the values are consistent with Poisson's ratio due to the in-plane compressive strain from the substrate. There is a significant change in the slope of the out-of-plane lattice parameter, *c*, close to 387 ºC because of the development of spontaneous polarization (ferroelectric transition) in the superlattice. Figure 4 also shows the in-plane and out-of-plane lattice parameters determined by the VTXRD on the superlattice of $[ST_4/BT_8]_{10}$. The discrepancy between our prediction and the VTXRD measurement for the lattice *c* is less than 0.41% over the whole temperature range, demonstrating an excellent agreement.

In summary, we studied the ferroelectricity and domain morphologies of BT/ST superlattices under different in-plane substrate constraints using the phase-field approach. We demonstrated that the coherency between a BT/ST superlattice film and its ST

substrate has a dramatic effect on the ferroelectricity of ST layers within the superlattice. It is an orthorhombic ferroelectric for a fully relaxed film while it exhibits only induced polarization by the adjacent BT layers for a fully commensurate or partially relaxed film. This work provides a consistent explanation of different conclusions in the literature with regard to the ferroelectricity of ST layers in BT/ST superlattices.

Acknowledgement

This work was partially supported by a Los Alamos National Laboratory Directed Research and Development Project under DOE, and by NSF under Grant Numbers: DMR-0122638, DMR-0507146, and ECS-0210449, and by DOE under DE-FG02-01ER45907.

[1] H. Tabata, H. Tanaka, and T. Kawai, Appl. Phys. Lett. **65,** 1970 (1994).

[2] Z. Y. Wang, T. Yasuda, S. Hatatani, and S. Oda, Jpn. J. Appl. Phys. Part 1 **38,** 6817 (1999).

[3] D. O'Neill, R. M. Bowman, and J. M. Gregg, Appl. Phys. Lett. **77,** 1520 (2000).

[4] J. Kim, Y. Kim, Y. S. Kim, J. Lee, L. Kim, and D. Jung, Appl. Phys. Lett. **80,** 3581 (2002).

[5] T. Shimuta, O. Nakagawara, T. Makino, S. Arai, H. Tabata, and T. Kawai, J. Appl. Phys. **91,** 2290 (2002).

[6] S. Rios, A. Ruediger, A. Q. Jiang, J. F. Scott, H. Lu, and Z. Chen, J. Phys.-Condes. Matter. **15,** L305 (2003).

[7] A. Q. Jiang, J. F. Scott, H. B. Lu, and Z. H. Chen, J. Appl. Phys. **93,** 1180 (2003).

[8] J. B. Neaton and K. M. Rabe, Appl. Phys. Lett. **82,** 1586 (2003).

[9] H. N. Lee, H. M. Christen, M. F. Chisholm, C. M. Rouleau, and D. H. Lowndes, Nature **434,** 792 (2005).

[10] L. J. Kim, J. Kim, D. G. Jung, and J. Lee, Appl. Phys. Lett. **87,** 052903 (2005).

[11] K. Johnston, X. Y. Huang, J. B. Neaton, and K. M. Rabe, Phys. Rev. B **71,** 100103 (2005).

[12] D. A. Tenne, A. Bruchhausen, N. D. Lanzillotti-Kimura, A. Fainstein, R. S. Katiyar, A. Cantarero, A. Soukiassian, V. Vaithyanathan, J. H. Haeni, W. Tian, D. G. Schlom, K. J. Choi, D. M. Kim, C. B. Eom, H. P. Sun, X. Q. Pan, Y. L. Li, L. Q. Chen, Q. X. Jia, S. M. Nakhmanson, K. M. Rabe, and X. X. Xi, Science **313,** 1614 (2006).

[13] Y. L. Li, S. Y. Hu, D. Tenne, A. Soukiassian, D. G. Schlom, X. X. Xi, K. J. Choi, C. B. Eom, A. Saxena, T. Lookman, Q. X. Jia, and L. Q. Chen, Appl. Phys. Lett. **91,** 112914 (2007).

[14] S. Lisenkov and L. Bellaiche, Phys. Rev. B **76,** 020102(R) (2007).

[15] Y. L. Li, S. Y. Hu, Z. K. Liu, and L. Q. Chen, Acta Mater. **50,** 395 (2002).

[16] Y. L. Li, S. Y. Hu, Z. K. Liu, and L. Q. Chen, Appl. Phys. Lett. **78,** 3878 (2001).

[17] A. K. Tagantsev, E. Courtens, and L. Arzel, Phys. Rev. B **64,** 224107 (2001).

[18] Y. L. Li, S. Choudhury, J. H. Haeni, M. D. Biegalski, A. Vasudevarao, A. Sharan, H. Z. Ma, J. Levy, V. Gopalan, S. Trolier-McKinstry, D. G. Schlom, Q. X. Jia, and L. Q. Chen, Phys. Rev. B **73,** 184112 (2006).

[19] K. H. Chew, Y. Ishibashi, F. G. Shin, and H. L. W. Chan, J. Phys. Soc. Jpn. **72,** 2364 (2003).

[20] A. L. Roytburd, S. Zhong, and S. P. Alpay, Appl. Phys. Lett. **87,** 092902 (2005).

TABLE I. Transition temperatures of superlattices determined from phase-field simulations and experimental measurements.

ST_4/BT_8	Phase-field simulations	UV Raman	VTXRD	Ferroelectric state of ST	Ferroelectric state of BT
Fully commensurate	387 ºC	365 ºC	400 ºC	Paraelectric with induced polarization	Tetragonal ferroelectric
Partially relaxed	166 ºC	167 ºC		Paraelectric with induced polarization	Tetragonal ferroelectric
Fully relaxed	170 ºC			Orthorhombic ferroelectric	Tetragonal ferroelectric

Captions of figures:

Fig. 1. (Color Online) In-plane lattice parameters of (001) ST substrate (a_{sub}) and superlattices ST_4/BT_8 (a_{sup}) under fully commensurate, partially relaxed, and fully relaxed conditions. The scattered squares and triangles represent the experimental data measured by VTXRD for superlattices of $[ST_4/BT_8]_{40}$ (partially relaxed) and $[ST_4/BT_8]_{10}$ (fully commensurate), respectively. The solid and dashed lines are the (pseudo-) cubic lattices of BT and ST crystals, respectively.

Fig. 2. (Color Online) Domain morphology of a fully relaxed superlattice of ST_4/BT_8 at room temperature.

Fig. 3. (Color Online) Distributions of the polarization components (P_1,P_2,P_3) across the superlattice thickness at room temperature under (a) fully commensurate, (b) partially relaxed, and (c) fully relaxed constraints, respectively.

Fig. 4. (Color Online) Unit cell lattice parameters versus temperature for the fully commensurate superlattice of ST_4/BT_8. The scatted symbols represent the data from experimental measurement by VTXRD on the superlattice of $[ST_4/BT_8]_{10}$. The solid lines are from the phase-field simulation.

FIG. 1.

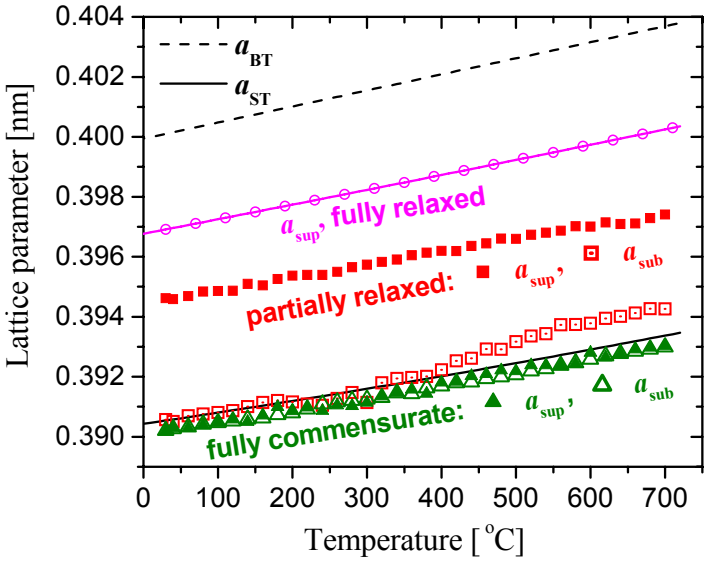

FIG. 2.

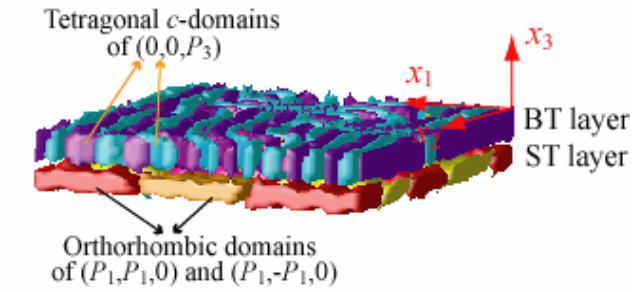

FIG. 3.

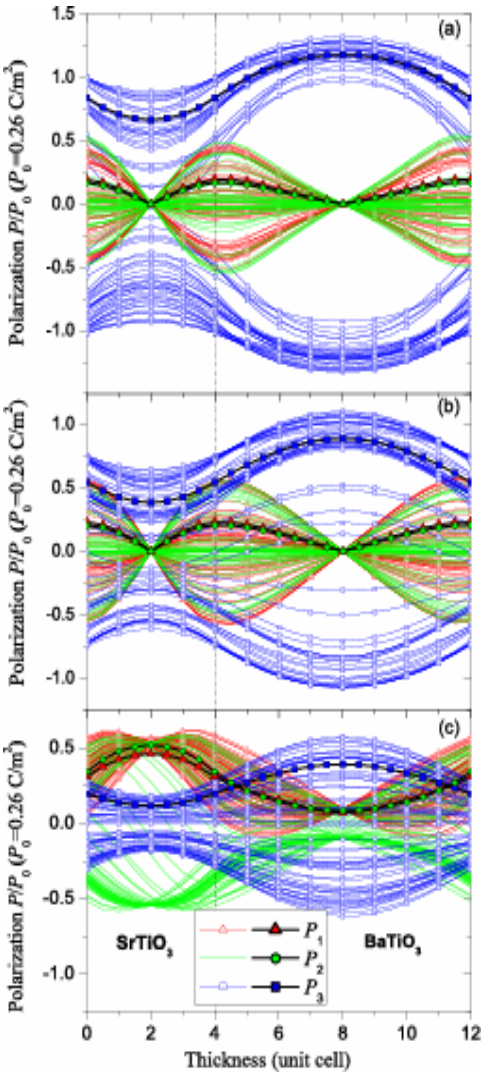

FIG. 4.